Bulletin of the Seismological Society of America, Vol. 93, No. 1, pp. 283–300, February 2003

Stability and Accuracy Analysis of Coarse-Grain Viscoelastic Simulations

by Robert W. Graves and Steven M. Day

Abstract We analyze the stability and accuracy of the coarse-grain memory variable technique used for viscoelastic wave-field simulations. Our analysis shows that the general behavior of the coarse-grain system is well described by effective parameters (M_E and Q_E) that are derived from the harmonic average of the moduli over the volume of the coarse-grain cell. The use of these effective parameters proves essential for analyzing the performance and accuracy of the coarse-grain system for Q values less than about 20. A necessary stability condition for the coarse-grain system requires that the weighting coefficients be bounded between 0 and 1. Specifying the weights using the approach of Day and Bradley (2001) satisfies this condition for Q values of about 3 and larger; however, using unconstrained optimization techniques will often produce weights that violate this condition at much higher Q values. We also derive a variation of the original coarse-grain methodology called the element-specific modulus (ESM) formulation in which each element of the coarse-grain cell uses a different unrelaxed modulus. We demonstrate that the accuracy of the coarse-grain system for Q values lower than about 20 is significantly improved with the ESM formulation without increasing the computational cost. Finally, we present a technique for optimizing the accuracy of the coarse-grain system for very low Q based on the use of the effective quality factor (Q_E). We demonstrate that using conventional optimization techniques that do not employ the effective parameter Q_E will actually degrade the accuracy of the coarse-grain system.

Introduction

The memory variable technique offers a powerful tool for the incorporation of anelasticity into time domain wave-field simulations (e.g., Day and Minster, 1984; Emmerich and Korn, 1987; Carcione *et al.*, 1988). This technique models a prescribed attenuation behavior by constructing a complex-valued modulus in the frequency domain using a linear combination of multiple relaxation mechanisms (e.g., Liu *et al.*, 1976). Transformation into the time domain yields a set of memory variables (one for each relaxation mechanism), which are updated using first-order differential equations. Increasing the number of relaxation mechanisms will increase the applicable bandwidth of the attenuation operator and will also improve the fit to the target attenuation model. In addition, to achieve the same degree of accuracy, models with strong attenuation (low Q) will generally require more relaxation mechanisms than models with weak attenuation (high Q). The drawback with using more relaxation mechanisms in the attenuation model is the large cost increase associated with updating and storing the additional memory variables. This is particularly burdensome for 3D applications where the use of more than just one or two discrete relaxation mechanisms can be very costly (e.g., Robertsson *et al.*, 1994; Xu and McMechan, 1998).

To address this issue, Day (1998) developed a coarse-graining methodology for memory variable calculations. In the coarse-grain approach, individual relaxation mechanisms are distributed in a spatially periodic manner across adjacent nodes of a finite-difference or finite-element grid. For 3D models, up to eight discrete relaxation mechanisms (one per grid node) can be accommodated in each coarse-grain cell. Using perturbation theory and verified by example, Day (1998) showed that the coarse-grain approach yields highly accurate results for $Q \gg 1$ as long as the wave field is sampled at a minimum of 4 points per wavelength. Furthermore, since only one relaxation mechanism is needed at each grid location, a tremendous reduction in storage and computational cost is realized. Recently, Day and Bradley (2001) have successfully extended the coarse-grain methodology to viscoelastic simulations.

The analyses of Day (1998) and Day and Bradley (2001) concentrate on the behavior of the coarse-grain system for constant (frequency independent) Q_0 values of 20 and greater. Using numerical examples, they find that the apparent Q measured from coarse-grain calculations matches the target Q_0 to within 4% tolerance over about two decades in frequency. While the range $Q > 20$ covers many seismological applications, recent studies illustrate the potential importance of considering even lower Q values. For example, Xu and McMechan (1998) cite Q values as low as 3 for shallow seismic reflection experiments, and Olsen *et al.*

(2001) require Q values as low as 10 for the modeling of long period ($T > 2$ sec) earthquake ground motions in the Los Angeles basin. Other applications using very low Q values include numerical dampers, such as sponge zones (Israeli and Orzag, 1981) that are used to reduce artificial reflections along computational boundaries. These applications stress the need to gain a better understanding of the coarse-grain system for low Q values.

Our approach here is to develop theoretical expressions that can be used to accurately describe the performance and behavior of the coarse-grain system, especially for low values of Q. We accomplish this by using effective parameters (M_{E} and Q_{E}), which are derived from the harmonic average of the viscoelastic moduli over the volume of the coarse-grain cell. These theoretical expressions predict that the behavior of the coarse-grain system begins to significantly deviate from that of the general (or non-coarse-grain) system when the target Q_0 value is less than about 20. This result has important implications for analyzing the accuracy of coarse-grain calculations and for developing improved formulations of the coarse-grain system.

In the sections that follow, we first provide a brief background of the memory variable approach and the coarse-grain implementation, including the specification of the effective parameters M_{E} and Q_{E}. Next, we derive a stability condition for the coarse-grain system and present an analysis of stability thresholds for optimized and nonoptimized systems. We show that optimized systems will generally violate the stability threshold at much larger Q values than the nonoptimized system. This is followed by a derivation of expressions for the unrelaxed (or infinite frequency) moduli using the element-specific modulus (ESM) formulation. This formulation assigns a different unrelaxed modulus to each relaxation mechanism and better represents the dispersive properties of the attenuating medium. We demonstrate through a series of example calculations that the ESM formulation provides improved accuracy relative to the conventional formulation, at virtually the same computational cost. In addition, we also show that the results of the ESM calculations are in very good agreement with the theoretical behavior of the coarse-grain system as predicted by the effective parameters M_{E} and Q_{E}. We then present a procedure for optimizing the accuracy of the coarse-grain system based on the use of Q_{E}, and we show that very good results are obtained even for Q values as low as 2. We conclude with a layered model comparison to demonstrate the effectiveness of the ESM formulation in the presence of sharp media interfaces (including a free surface) and then we discuss some practical considerations of applying the coarse-grain system in generally heterogeneous 3D media.

Viscoelastic Modulus Representation

In the frequency domain, a general viscoelastic modulus $M(\omega)$ can be approximated using a discrete relaxation spectrum as

$$M(\omega) = M_u\left[1 - \frac{\delta M}{M_u}\sum_{j=1}^{N}\frac{a_j}{i\omega\tau_j + 1}\right], \qquad (1)$$

where M_{u} is the unrelaxed modulus, $\frac{\delta M}{M_u}$ is the modulus reduction factor, τ_j are relaxation times ($\tau_j = 1/\omega_j$), a_j are coefficients chosen to fit a desired spectrum, and $i = (-1)^{1/2}$ is the imaginary unit. Equation (1) follows from either equation (25) of Day and Minster (1984) or equation (11) of Emmerich and Korn (1987). Using equation (1), the quality factor is given by

$$Q(\omega) \equiv \frac{\mathrm{Re}[M(\omega)]}{\mathrm{Im}[M(\omega)]} = \frac{1 - \frac{\delta M}{M_{\mathrm{u}}}\sum_{j=1}^{N}\frac{a_j}{\omega^2\tau_j^2 + 1}}{\frac{\delta M}{M_{\mathrm{u}}}\sum_{j=1}^{N}\frac{a_j\omega\tau_j}{\omega^2\tau_j^2 + 1}}. \qquad (2)$$

In the general application of the memory variable method, given a target $Q(\omega)$, the coefficients a_j and τ_j can be prescribed using Padé approximants (Day and Minster, 1984) or simple approximation formulas (e.g., Day and Bradley, 2001), or alternatively, equation (2) can be used to numerically solve for the coefficients a_j and τ_j (e.g., Emmerich and Korn, 1987; Xu and McMechan, 1998). Once the a_j and τ_j are set, equation (1) can be used to derive the viscoelastic-wave equations and associated memory variable equations (N equations in all), which then must be solved at each computational node in the model grid (for details, see Emmerich and Korn, 1987; Robertsson *et al.*, 1994; Xu and McMechan, 1998).

Coarse-Grain Implementation

Without loss of generality, we can rewrite equation (1) as

$$M(\omega) = M_{\mathrm{u}}\left[1 - \sum_{j=1}^{N}\frac{x_j}{i\omega\tau_j + 1}\right], \qquad (3)$$

where we have set

$$x_j = \frac{\delta M}{M_u}a_j. \qquad (4)$$

In the coarse-grain approach, the N memory variables associated with equation (3) are distributed over N adjacent grid elements of the discrete simulation model, so that there is only one memory variable for each grid element (Day, 1998; Day and Bradley, 2001). This implies that each grid element has its own discrete viscoelastic modulus given by

$$M_k(\omega) = M_{k_u}\left[1 - \frac{\bar{x}_k}{i\omega\tau_k + 1}\right], \qquad (5)$$

where $k = 1, \ldots, N$ in the periodic manner described by Day (1998), M_{k_u} is the element specific unrelaxed modulus, and

$$\bar{x}_k = \frac{V_T}{V_k} x_k \tag{6}$$

are the volumetric normalized coefficients, with the volume of the kth grid element given by V_k and the total volume of the N adjacent grid elements given by $V_T = \sum_{j=1}^{N} V_j$.

The coarse-grain theory developed by Day (1998) states that for wavelengths longer than about 4 grid elements and for $Q \gg 1$, the application of equation (5) at N adjacent grid elements will yield a good approximation to the general relaxation spectrum given by equation (1) and thus will satisfactorily reproduce the attenuation behavior predicted by equation (2).

However, as will be shown later, the general behavior of the coarse-grain system is actually better described not by the general modulus given in equation (1), but rather by the effective modulus that is derived from the harmonic average of the $M_k(\omega)$ over the volume of the coarse-grain cell. We define this effective modulus as $M_{\mathrm{E}}(\omega)$, which is given by

$$M_{\mathrm{E}}(\omega) = V_T \left[\sum_{k=1}^{N} \frac{V_k}{M_k(\omega)} \right]^{-1}, \tag{7}$$

with an associated effective quality factor $Q_{\mathrm{E}}(\omega)$ given by

$$Q_{\mathrm{E}}(\omega) = \frac{\mathrm{Re}[M_{\mathrm{E}}(\omega)]}{\mathrm{Im}[M_{\mathrm{E}}(\omega)]}. \tag{8}$$

More complete expressions for $M_{\mathrm{E}}(\omega)$ and $Q_{\mathrm{E}}(\omega)$ are given in the Appendix. Our use of harmonic averaging to define effective parameters follows from analogous formulations used to precisely represent media heterogeneity in grid based calculations (e.g., Zahradník *et al.*, 1993; Graves, 1996; Moczo *et al.*, 2001). In the next section, we show that for target Q values greater than about 20, there is little difference between the effective modulus given by equation (7) and the general modulus given by equation (1). However, for smaller values of Q, the difference becomes quite significant, and it is shown that the behavior of the coarse-grain system follows very closely the theoretical behavior predicted by these effective parameters. Thus, these effective parameters provide a general framework for analyzing and optimizing the accuracy of the coarse-grain system, particularly for low values of Q.

Stability Analysis

To ensure physical stability for any viscoelastic modulus, two necessary conditions must be satisfied. First, the modulus at zero frequency (relaxed modulus) must remain strictly positive, and second, the general viscoelastic modulus must be dissipative for all frequencies. The first condition follows from thermodynamic considerations of Hooke's law, and the second condition places a positivity constraint on the quality factor (negative values would give rise to energy amplification, not dissipation). Satisfying both of these conditions using the discrete relaxation spectrum formulation requires that both the real and imaginary parts of the spectrum remain positive.

Starting with equation (5), we rewrite this expression into its discrete real and imaginary parts, giving

$$M_k(\omega) = M_{k_u}\left[1 - \frac{\bar{x}_k}{\omega^2\tau_k^2 + 1} + i \frac{\bar{x}_k \omega \tau_k}{\omega^2\tau_k^2 + 1} \right]. \tag{9}$$

Visual inspection of equation (9) leads to the following stability condition

$$0 \le \frac{\bar{x}_k}{\omega^2\tau_k^2 + 1} < 1, \tag{10}$$

which, since this must hold for all $\omega^2 \ge 0$, can be simplified to

$$0 \le \bar{x}_k < 1. \tag{11}$$

Equation (11) represents a necessary stability condition for the memory variable system, and it must be satisfied regardless of how the $\bar{x}_k$ and τ_k coefficients are determined.

In satisfying this stability condition, there exists a tradeoff between the absorption bandwidth over which the prescribed relaxation spectrum is valid and the accuracy to which this relaxation spectrum matches the desired Q model. Furthermore, given a prescribed absorption bandwidth, there will generally be some minimum value of the desired Q model below which the stability condition will be violated. For example, Day (1998) and Day and Bradley (2001) assume a frequency-independent Q model and use a simple procedure to set all of the coefficients $\bar{x}_k$ in the coarse-grain system equal to the same constant value

$$\bar{x}_k = \frac{\delta M}{M_{\mathrm{u}}} \approx \frac{2 \ln(\tau_M/\tau_0)}{[\pi Q_0 - 2 \ln(\omega_0\tau_0)]}, \tag{12}$$

with the τ_k evenly distributed on a logarithmic scale

$$\ln\tau_k = \ln \tau_0 + \frac{2k - 1}{2N} [\ln(\tau_M/\tau_0)] \quad k = 1, \ldots, N. \tag{13}$$

Here, τ_0 and τ_M are the lower and upper absorption-band cutoffs, and ω_0 is a prescribed reference frequency where the resulting relaxation spectrum matches the desired constant Q_0. Setting $\omega_0 = (\tau_M\tau_0)^{-1/2}$ (i.e., the geometric average of the absorption-band cutoffs), inserting equation (12)

into the stability condition (11) and rearranging terms, we get

$$-\pi Q_0 \leq \ln(\tau_M/\tau_0) < \pi Q_0. \tag{14}$$

By definition $\tau_M > \tau_0$, thus the lower bound condition will always be satisfied with this simple parameterization. However, for a given τ_M and τ_0, there will always be a minimum (positive) Q_0 below which the upper bound condition will be violated. For example, using numerical experiments, Day (1998) showed that the relation $\tau_M/\tau_0 = 10^4$ provides a nearly frequency-independent Q (for $Q \geq 20$) over more than two decades of bandwidth. Inserting this value into equation (10), we have the requirement $Q_0 > \ln(10^4)/\pi \approx 3$.

Figure 1 plots the resulting $Q(\omega)$ and $Q_E(\omega)$ obtained from equations (2) and (A6) respectively, using the above coefficient parameterization (i.e., equations 12 and 13) with $N = 8$, and various target values of Q_0. Also shown on this plot are the values of $\bar{x}_k$ associated with each Q_0. This plot clearly shows that as the target Q_0 decreases, the approximation provided by the above parameterization becomes increasingly less accurate. In addition, as Q_0 decreases, the $\bar{x}_k$ coefficients increase, with the value at $Q_0 = 2$ exceeding the stability limit. This figure also shows that the effective quality factor $Q_E(\omega)$ provides a less accurate fit to the target Q_0 than the general quality factor $Q(\omega)$ that would result from a non–coarse-grain implementation. For this parameterization, the difference between $Q(\omega)$ and $Q_E(\omega)$ is only significant for Q_0 less than about 10. Numerical simulations are in agreement with this theoretical behavior.

In theory, more accurate representations of $Q(\omega)$ can be obtained by optimizing the $\bar{x}_k$ and τ_k using numerical techniques (e.g., Emmerich and Korn, 1987; Xu and McMechan, 1998). Although these optimization procedures can provide a very accurate match to the general $Q(\omega)$ over a specified bandwidth, they will generally produce $\bar{x}_k$ that will violate the coarse-grain stability condition (11) at a much higher target Q value than when using a simpler approximation. Furthermore, the effective quality factor of the coarse-grain system $Q_E(\omega)$ obtained from these types of optimization procedures can be very different from the general $Q(\omega)$.

We demonstrate this behavior by using the least-squares algorithm of Emmerich and Korn (1987) to solve for the coefficients $\bar{x}_k$ for various values of Q_0. Again, the τ_k were prescribed using the relation of Day and Bradley (2001) and we set $\tau_M/\tau_0 = 10^4$ and $N = 8$. Figure 2 plots the resulting $Q(\omega)$ and $Q_E(\omega)$ for this parameterization, and various values of Q_0. Also shown are the maximum of the $\bar{x}_k$ coefficients obtained for each Q_0. Clearly, the match to the general attenuation model $Q(\omega)$ is quite accurate even for very small values of Q_0. However, the maximum of the $\bar{x}_k$ coefficients increases quite rapidly with decreasing Q_0, and exceed the stability limit at about $Q_0 = 10$. In addition, as Q_0 decreases, the effective quality factor $Q_E(\omega)$ begins to diverge quite significantly from the general $Q(\omega)$. Since it is the $Q_E(\omega)$ that governs the attenuation behavior of the coarse-grain method, optimizing the fit to the general $Q(\omega)$ will actually degrade the accuracy of the coarse-grain system. This behavior will be demonstrated later by example, and we will subsequently exploit this fact to show that improved accuracy can be obtained by optimizing directly on $Q_E(\omega)$ instead of on $Q(\omega)$.

Specification of the Element-Specific Unrelaxed Modulus

Day and Bradley (2001) give an expression for the unrelaxed modulus based on the constant Q_0 model, and they assume that the unrelaxed modulus (M_u) is the same at all of the N adjacent grid elements in the coarse-grain system. For Q_0 greater than about 20, this approach works reasonably well. However, this formulation equalizes the element-specific phase velocities at infinite frequency. Since each relaxation mechanism gives rise to a different dispersion relation, the result is to induce small-scale heterogeneity in the phase velocity at those frequencies that fall within or below the absorption band. The performance of the method is improved, especially at very low Q, if we instead minimize the phase-velocity heterogeneity at some reference frequency falling near the center of the band of computational interest. We can accomplish this by permitting the element-specific unrelaxed moduli (M_{k_u}) to vary within the coarse-grain cell in such a way as to equalize the element specific frequency-dependent moduli at the reference frequency.

Following Kjartansson (1979), the phase velocity in an attenuating medium is given by

$$c^{-1}(\omega) = \mathrm{Re}\left[\left(\frac{\rho}{M(\omega)}\right)^{1/2}\right], \tag{15}$$

where ρ is the medium density. Inserting the element-specific modulus (equation 9) for the modulus in equation (15), and then evaluating the resulting expression at a reference frequency $f_0 = \omega_0/2\pi$, we get (after rearranging terms)

$$M_{k_u} = c_0^2\, \rho\, \frac{1}{2}\, [A_{k_0}^2 + B_{k_0}^2]^{-1/2} \{1 + A_{k_0}\, [A_{k_0}^2 + B_{k_0}^2]^{-1/2}\}, \tag{16}$$

where

$$A_{k_0} = 1 - \frac{\bar{x}_k}{\omega_0^2\tau_k^2 + 1} \quad \text{and} \quad B_{k_0} = \frac{\bar{x}_k \omega_0 \tau_k}{\omega_0^2\tau_k^2 + 1}, \tag{17}$$

and c_0 is the prescribed propagation velocity at the reference frequency.

Equation (16) can be interpreted as a prescription for a set of element-specific unrelaxed moduli M_{k_u} that ensure spatial homogeneity (i.e., over the coarse-grain cell) of the mod-

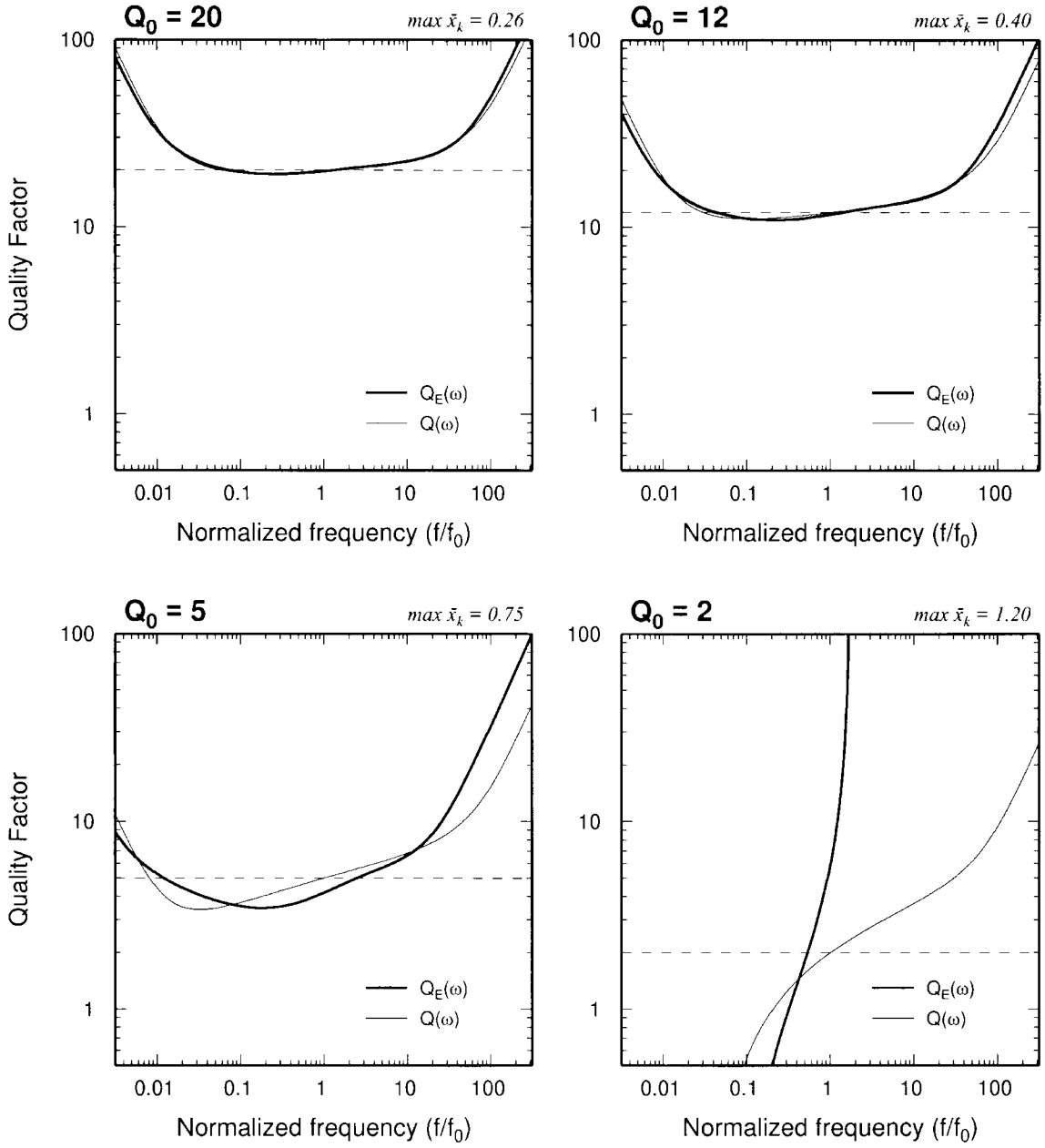

Figure 1. Plots of $Q(\omega)$ (thin line, from equation 2) and $Q_E(\omega)$ (thick line, from equation A6) determined using the formulation of Day and Bradley (2001) to specify the $\bar{x}_k$ coefficients for various target values of Q_0. The maximum $\bar{x}_k$ for each Q_0 is shown at the upper right of each panel.

ulus at the reference frequency f_0. This equation has two important implications. First, even if the reference medium is entirely homogeneous, this expression requires that the N adjacent grid elements in the coarse-grain system each have a different elastic (unrelaxed) modulus. However, this apparent heterogeneity will exist only at very short wavelengths (and high frequencies). The above parameterization will provide a good approximation to the frequency-dependent modulus as long as the propagation wavelengths are about 4 grid elements or greater (consistent with the coarse-grain theory developed by Day [1998]). For low-order finite-difference (FD) and finite-element (FE) implementations, this condition is easily satisfied.

The second implication of using equation (16) is that the maximum allowable timestep will be controlled by the largest M_{k_u} in the entire model domain, which will always be larger than the corresponding effective M_u. This effect might be significant, particularly when low values of Q_0 occur in the highest velocity portions of the model. Fortunately, the lowest Q values tend to strongly correlate with

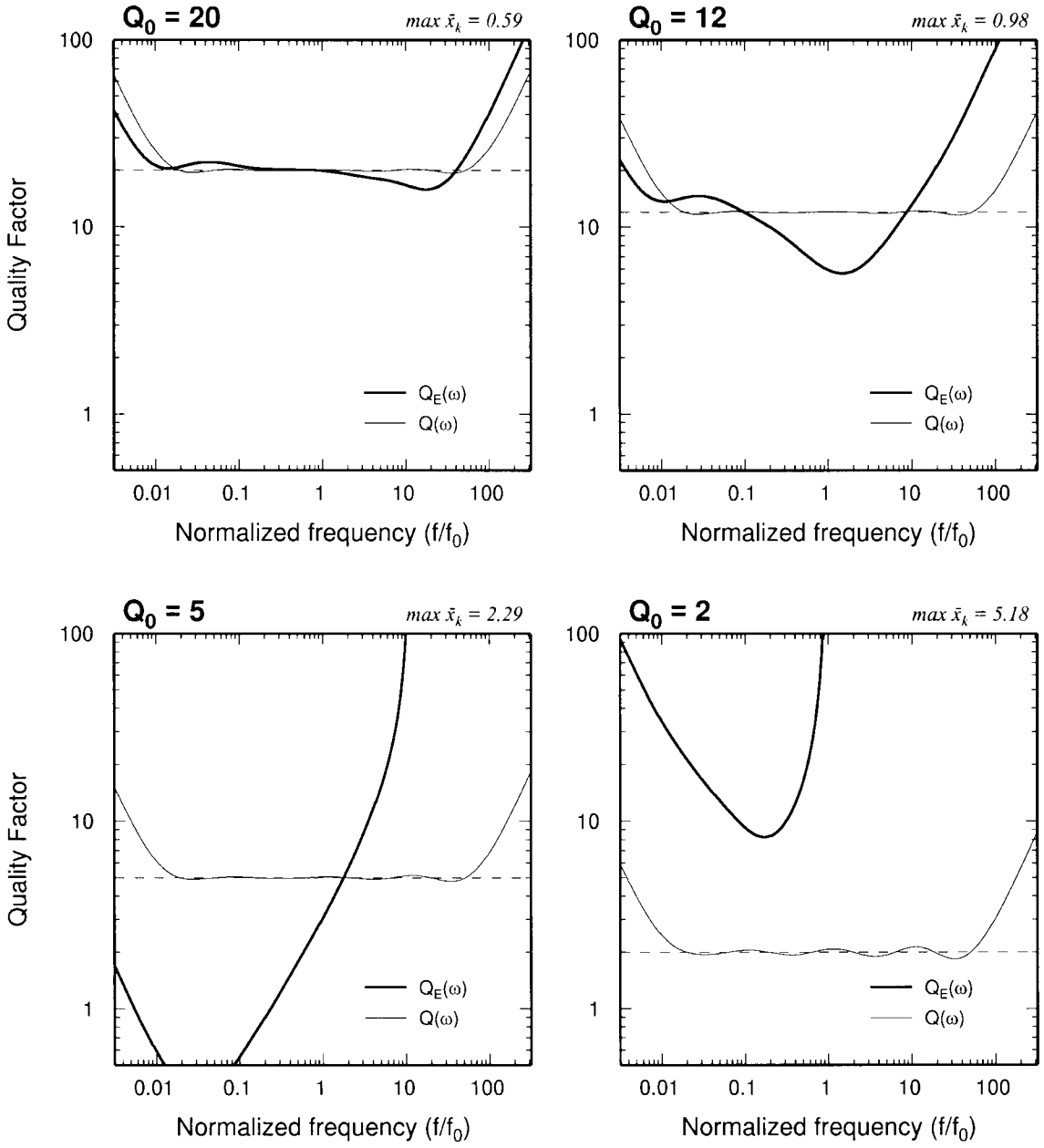

Figure 2. Plots of $Q(\omega)$ (thin line, from equation 2) and $Q_E(\omega)$ (thick line, from equation A6) determined using the least-squares formulation of Emmerich and Korn (1987) to specify the $\bar{x}_k$ coefficients for various target values of Q_0. The maximum $\bar{x}_k$ for each Q_0 is shown at the upper right of each panel.

the lowest velocities, so the overall impact of this second effect is generally not significant.

To demonstrate the importance of using the element specific modulus given by equation (16), we have performed a series of numerical calculations using a 3D staggered-grid FD code (Graves, 1996). These calculations use plane-wave models similar to that used by Day (1998) and Day and Bradley (2001). The calculations are initiated by imposing a velocity pulse with shape $s(t) = t \exp(-t/T)$ along one plane of the 3D grid. Motion is specified either normal (P wave) or parallel (S wave) to the plane. The medium is a whole space with P- and S-wave velocities of 6 km/sec and 3.46 km/sec, respectively, prescribed at a reference frequency of $f_0 = 1$ Hz and a density of 2.7 g/cm^3.

We use a constant Q model and set the $\bar{x}_k$ and τ_k coefficients using equations (12) and (13). Two values of Q_0 are considered, 20 and 5, and the associated τ_0, τ_M, f_0 and c_{max} (maximum propagation velocity as determined from equation 16), are shown in Table 1. These values of τ_0 and τ_M give a target bandwidth for the constant Q_0 model of about four decades (roughly 0.01–100 Hz). While these Q values are much lower than might be expected for the prescribed

Table 1
Attenuation Parameters for Plane-Wave Tests

Q_o	τ_o	τ_M	f_o(Hz)	c_{max}(km/sec)
20	0.00159	15.9	1.0	6.97
5	0.00159	15.9	1.0	11.87

seismic velocities, this model is useful for demonstrating the performance of the technique. In a later section, we will consider a model with a more realistic layered velocity structure. For all calculations, the source duration parameter T is set to 0.1, and the grid spacing is 0.1 km.

Figure 3 plots the velocity waveforms simulated at a propagation distance of 10 km for each of the previous cases. At the characteristic source duration T, this propagation distance corresponds to about 16 wavelengths for P waves and about 29 wavelengths for S waves. The analytic solution is computed using the formulation of Kjartansson (1979). We used two different formulations to specify the unrelaxed modulus in the FD simulations. The first (labeled *Element-Specific* M_{k_u} and hereafter referred to as the ESM formulation) uses equation (16) to determine the element-specific unrelaxed modulus for each of the 8 adjacent grid elements in the coarse-grain system. The second (labeled *Constant* M_u and hereafter referred to as the CM formulation) uses the method of Day and Bradley (2001) to determine a single unrelaxed modulus, which is then used for all grid elements in the entire model. In all cases, the velocity pulse is normalized to unit amplitude at zero distance. Thus, for a purely elastic medium (Q = infinity), the amplitude of the velocity pulse would remain at unity for all propagation distances.

For $Q_0 = 20$, the ESM formulation gives an excellent match to the timing, waveform, and amplitude of the analytic time history for both P and S waves. The CM formulation produces a very good result for this Q_0 value as well, with the only noticeable shortcoming being a slight phase delay of the pulse. At $Q_0 = 5$, the difference in performance between the two formulations is much more significant, with the ESM formulation clearly providing a better overall match to the analytic response. Although both formulations underpredict the amplitude of the analytic pulse, the CM response also exhibits a significant phase delay.

Taking the response at two locations separated by a distance Δx, we can measure the apparent Q from these plane-wave tests using the relation

$$Q_A^{-1}(\omega) = -2\,\frac{c(\omega)}{\omega \Delta x}\left[\ln|v(x+\Delta x,\omega)| - \ln|v(x,\omega)|\right], \tag{18}$$

where $|v(x,\omega)|$ is the Fourier amplitude spectrum of the velocity time history at location x and the frequency-dependent phase velocity $c(\omega)$ is given by (Kjartansson, 1979)

$$c(\omega) = c_0 \left|\frac{\omega}{\omega_0}\right|^{\gamma} \left[\cos\left(\frac{\pi\gamma}{2}\right)\right]^{-1}, \tag{19}$$

with c_0 the specified velocity at reference frequency f_0 and

$$\gamma = \frac{1}{\pi}\tan^{-1}\left[\frac{1}{Q_0}\right]. \tag{20}$$

Equation (18) differs slightly from the relation used by Day and Bradley (2001) in that we use $c(\omega)$ instead of the constant c_0. The form used here gives more accurate results for low Q values.

Figure 4 plots the Q_A computed for each of the above plane-wave calculations at a separation distance of $\Delta x = 2$ km. These results are plotted up to 12 Hz for P waves and 7 Hz for S waves, which corresponds to a sampling of 5 grid points per respective wavelength. The low-frequency cutoff for the results is determined by the total computed duration, which is generally about 12–15 sec.

For $Q_0 = 20$, both formulations do reasonably well at matching the desired Q behavior over roughly two decades of frequency (centered at the reference value of 1 Hz). As discussed by Day (1998) and demonstrated by the results in Figure 4, the accuracy of the coarse-grain method begins to diminish near the 5 grid points per wavelength sampling limit. For $Q_0 = 5$, the accuracy of both formulations is reduced relative to the higher Q_o case. However, the ESM formulation still matches the target Q_0 value to about $\pm 25\%$ over the central two-decade frequency band, whereas the CM formulation significantly underpredicts the target Q_0 over most of this same bandwidth.

Also shown in the panels of Figure 4 are the coarse-grain effective Q curves $[Q_E(\omega)]$ given by equation (A6). In each case, the ESM formulation follows the theoretical behavior of the $Q_E(\omega)$ curve reasonably well, particularly for frequencies above 1 Hz. At lower frequencies, the ESM results deviate somewhat from the theoretical curves (most noticeable for the S wave case at low Q). We suspect that this deviation is caused by (very low amplitude) artificial boundary reflections, which are virtually impossible to suppress completely from the calculations. The importance of considering the $Q_E(\omega)$ behavior will be discussed further in the following section.

As a final comparison, we have computed the P- and S-wave phase velocities for each of the plane-wave calculations, and these results are plotted in Figure 5. The phase velocity is obtained by measuring the phase delay of each Fourier component in the computed time history at two adjacent locations (1 km apart in this case). In the plots shown in Figure 5, we have normalized the measured phase velocity by the theoretical value given by equation (19), thus a value of one gives an exact match to the analytic result.

For $Q_0 = 20$, the ESM formulation provides a very close match to the theoretical result across roughly two decades of frequency. The CSM formulation produces a phase ve-

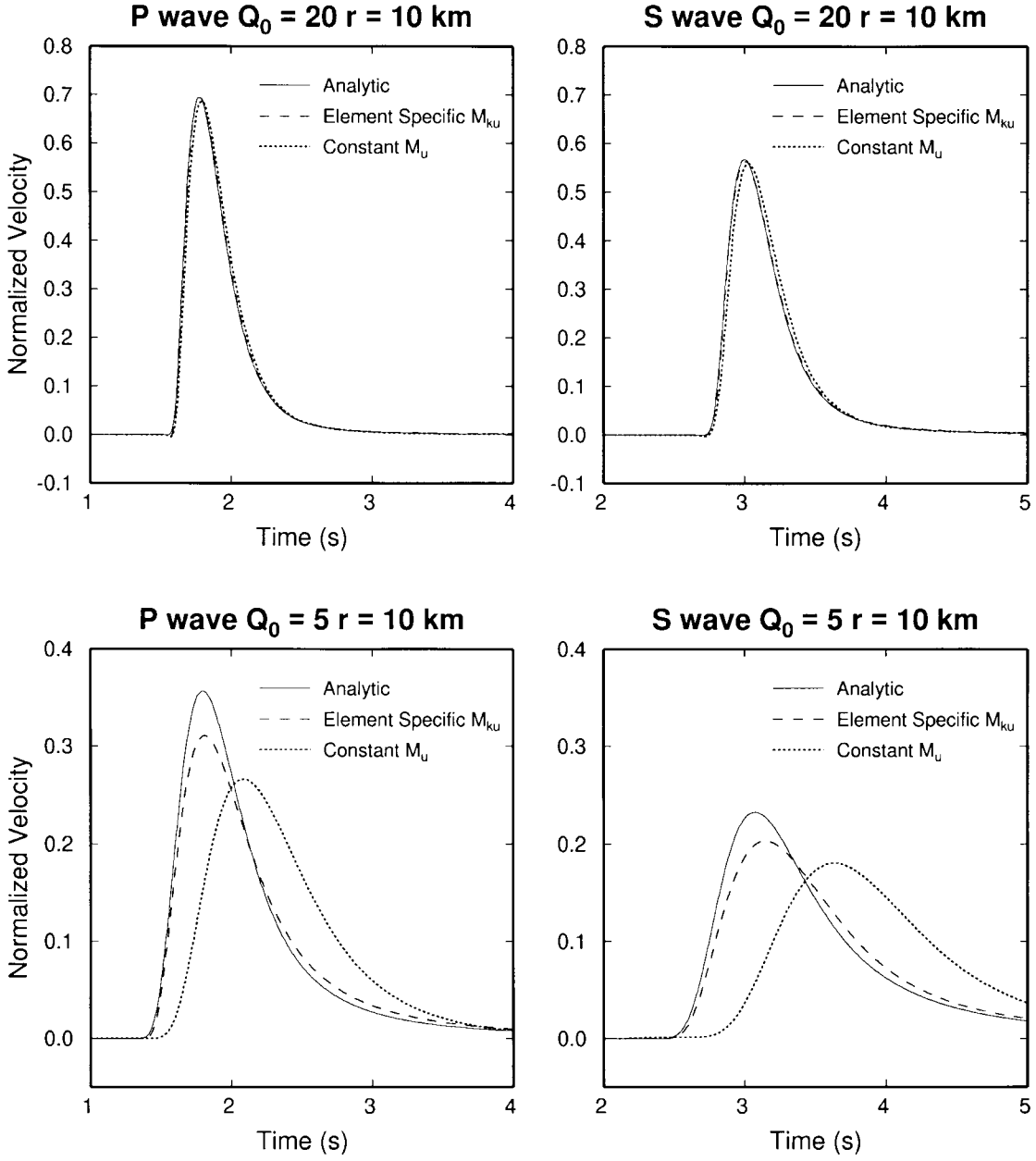

Figure 3. Waveform comparison for plane *P*-wave (left panels) and *S*-wave (right panels) calculations with target Q_0 values of 20 (upper panels) and 5 (lower panels). Propagation distance is 10 km. The analytic solution (solid line) is from Kjartansson (1979). For the coarse-grain calculations, the element-specific M_{k_u} solution (dashed line) uses equation (16) to specify the unrelaxed moduli and the constant M_u solution (dotted line) uses the method of Day and Bradley (2001) to specify the unrelaxed modulus. Both coarse-grain solutions use the method of Day and Bradley (2001) to specify the $\bar{x}_k$ and τ_k coefficients.

locity that is about 1% less than the theoretical value over this same bandwidth. This result is consistent with the observed phase delay seen in Figure 3. For $Q_0 = 5$, both formulations exhibit significant dispersion relative to the theoretical value; however, the ESM formulation clearly provides a more accurate result. The largest mismatch of the ESM formulation is on the order of a few percent and occurs at the lower frequencies. In the time domain, this is manifest by a slight delay of the waveform tails as seen in the lower panels of Figure 3. On the other hand, the CM formulation underpredicts the theoretical value by roughly 10% over most of the bandwidth, resulting in a noticeable delay of the

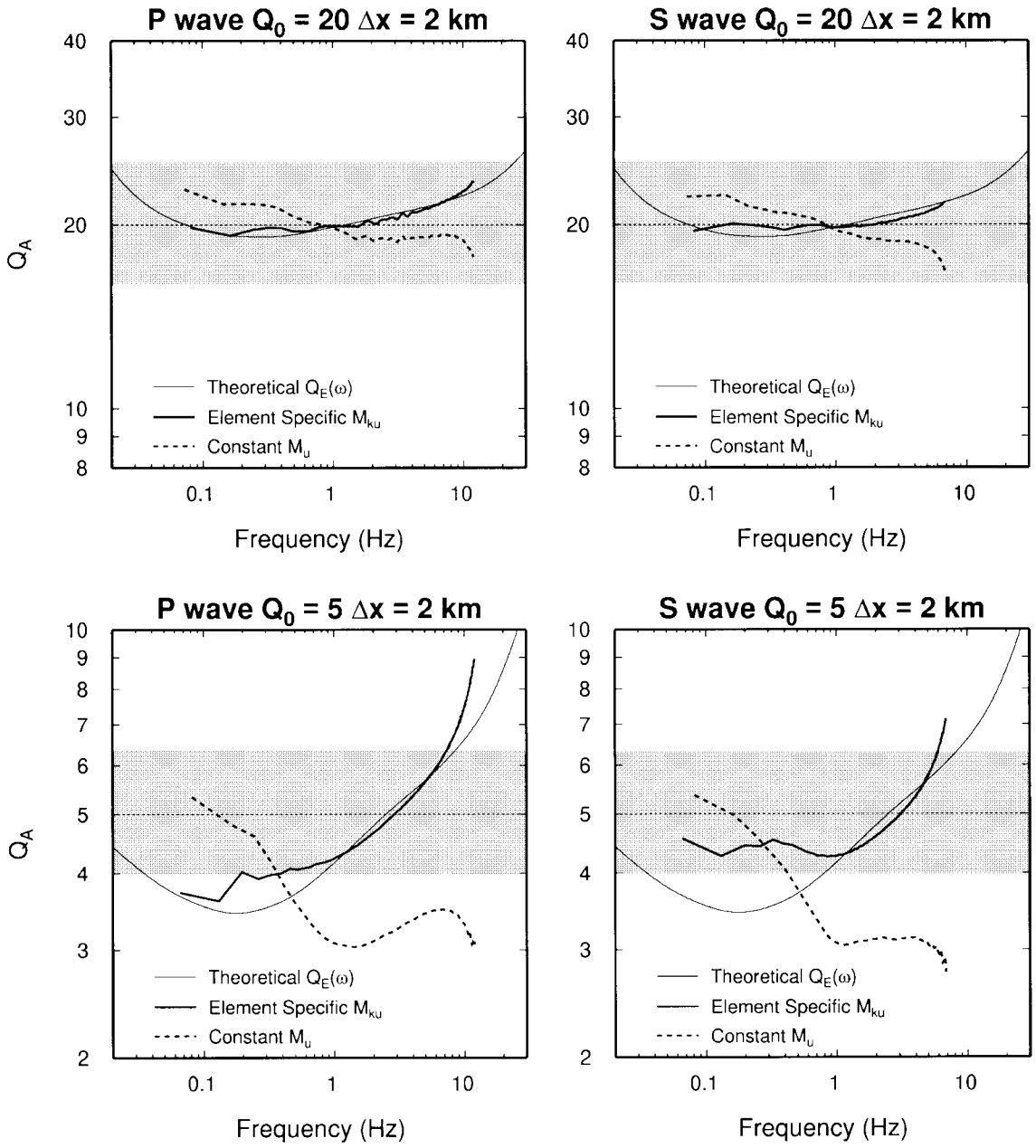

Figure 4. Apparent attenuation (Q_A) for the plane *P*-wave (left panels) and *S*-wave (right panels) calculations with target Q_0 values of 20 (upper panels) and 5 (lower panels). Separation distance is 2 km. The shaded region represents $\pm 25\%$ variation around the target Q_0 value. For the coarse-grain calculations, the element-specific M_{k_u} solution (thick line) uses equation (16) to specify the unrelaxed moduli and the constant M_u solution (dashed line) uses the method of Day and Bradley (2001) to specify the unrelaxed modulus. Both coarse-grain solutions use the method of Day and Bradley (2001) to specify the $\bar{x}_k$ and τ_k coefficients. Also shown are theoretical $Q_E(\omega)$ curves determined from equation (A6).

entire waveform pulse as shown in Figure 3. Also shown in this figure are the effective phase velocity curves $c_E(\omega)$, which we have derived from the effective modulus $M_E(\omega)$ using equation (15). For each case, the behavior of the ESM calculation is predicted nicely using the theoretical $c_E(\omega)$ curves.

Significance of Effective Parameters M_E and Q_E

The importance of using the effective parameters M_E and Q_E to analyze the behavior of the coarse-grain system is further demonstrated by the results shown in Figure 6. Here, we approximate a constant Q_0 of 12 with the general $Q(\omega)$ given by equation (2) and solve for the $\bar{x}_k$ coefficients

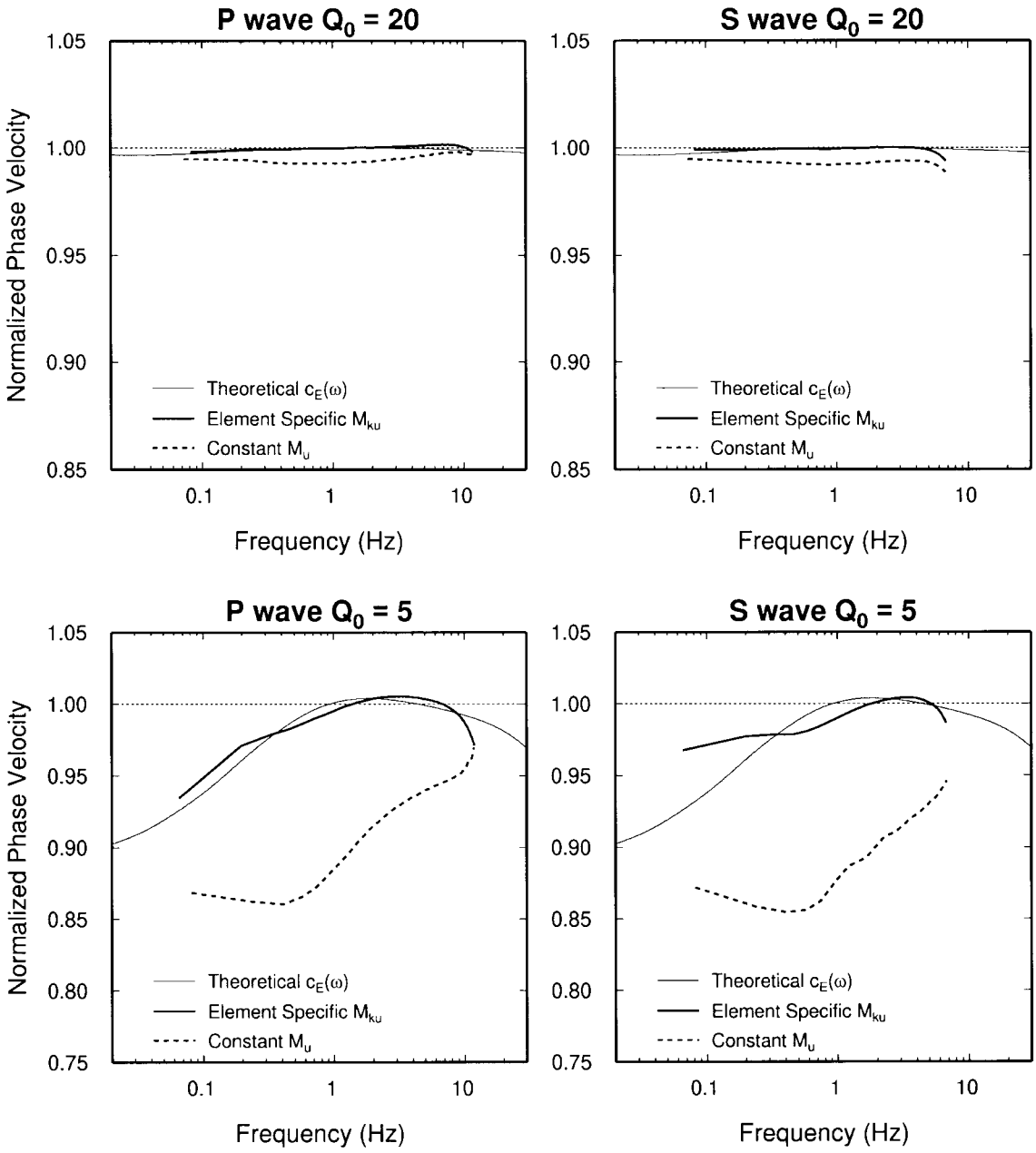

Figure 5. Normalized phase velocity measured from the plane *P*-wave (left panels) and *S*-wave (right panels) calculations with target Q_0 values of 20 (upper panels) and 5 (lower panels). For the coarse-grain calculations, the element-specific M_{k_u} solution (thick line) uses equation (16) to specify the unrelaxed moduli and the constant M_u solution (dashed line) uses the method of Day and Bradley (2001) to specify the unrelaxed modulus. Both coarse-grain solutions use the method of Day and Bradley (2001) to specify the $\bar{x}_k$ and τ_k coefficients. Also shown are theoretical $c_E(\omega)$ curves determined from equations (15) and (A5).

using the least-squares algorithm of Emmerich and Korn (1987). The τ_k are the same as in the preceding calculations, and we use the ESM formulation. As shown in Figure 2, this parameterization gives a maximum $\bar{x}_k$ that is just within the stability threshold for the coarse-grain system. Figure 6 compares the theoretical and computed waveforms, apparent attenuation (Q_A), and measured phase velocity for this formulation. Here, we only show results for *P* waves, although very similar results are obtained for *S* waves.

As discussed earlier (Fig. 2), the theoretical behavior of the general $Q(\omega)$ for the least-squares formulation matches the constant Q_0 of 12 very well over nearly 4 decades of frequency. For a non–coarse-grain system, we would expect this parameterization to produce numerical results that

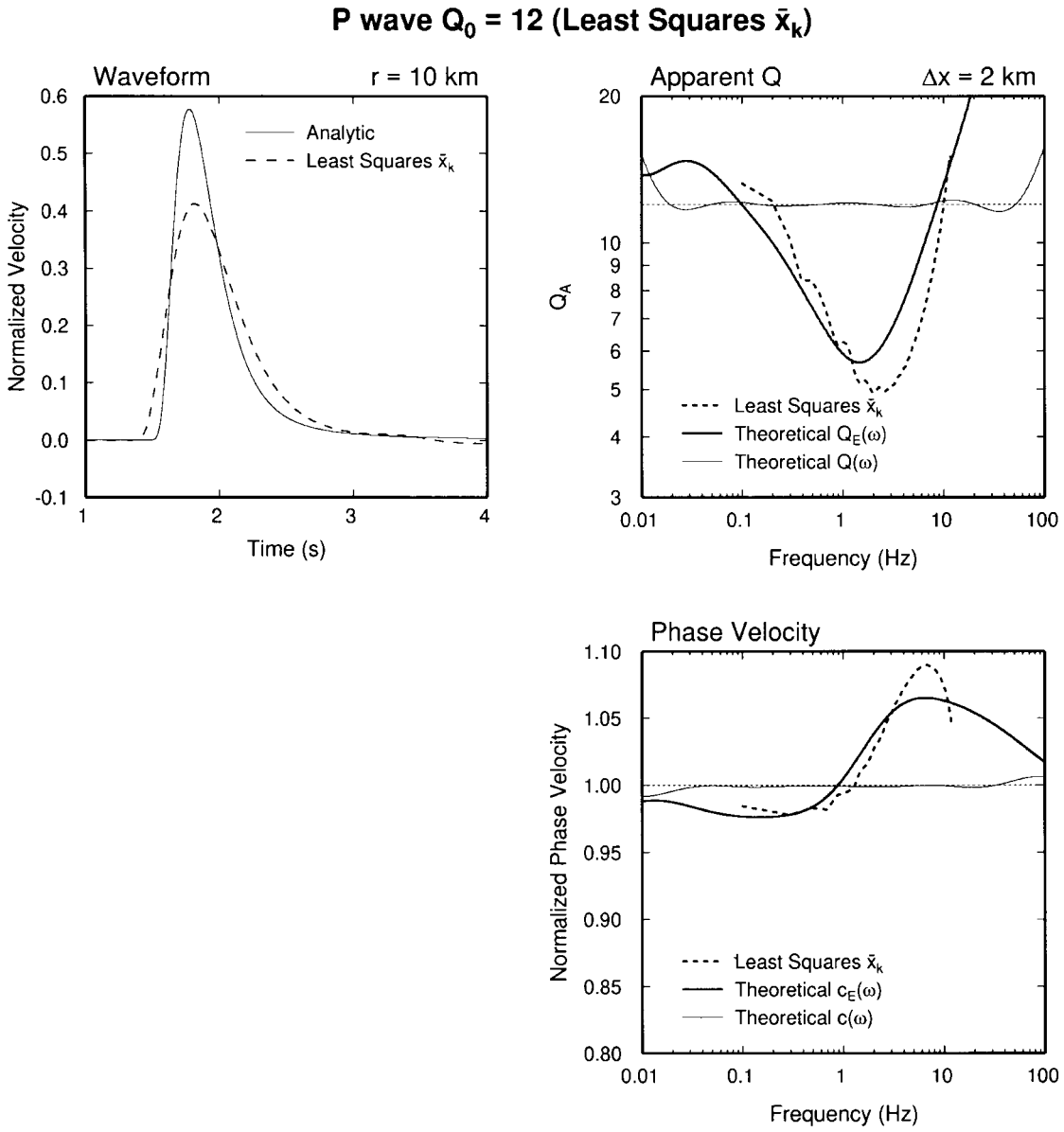

Figure 6. Theoretical and calculated waveform (upper left), Q_A (upper right) and phase velocity (lower right) comparisons for the plane *P*-wave model with $Q_0 = 12$, and using the least-squares approach of Emmerich and Korn (1987) to determine the $\bar{x}_k$ coefficients. Theoretical curves for the general [$Q(\omega)$ and $c(\omega)$] and effective [$Q_E(\omega)$ and $c_E(\omega)$] parameters are included in the right panels.

closely follow this predicted theoretical behavior. However, the comparisons in Figure 6 clearly show that when used in the coarse-grain system, the least-squares parameterization actually produces very poor results. The reason for this is that the behavior of the coarse-grain system is more accurately described by the effective parameters, $Q_E(\omega)$ and $c_E(\omega)$, which for this case, are quite different than the general parameters $Q(\omega)$ and $c(\omega)$. The apparent attenuation and phase velocity plots in Figure 6 illustrate the nice agreement between the theoretical curves for $Q_E(\omega)$ and $c_E(\omega)$ and the computed response. This example highlights the pitfalls in using the general $Q(\omega)$ to determine the choice of the $\bar{x}_k$ coefficients for the coarse-grain system, since the accuracy of resulting parameterization may actually be significantly degraded.

Improved Accuracy and Stability for Low Q_0

The results from the preceding section suggest that a better approach for improving the accuracy of the coarse-grain system is to use the effective parameter $Q_E(\omega)$ instead of the general $Q(\omega)$ to guide the determination of the $\bar{x}_k$ and τ_k coefficients (e.g., by optimizing the fit to the target Q_0).

The relationship among the $\bar{x}_k$, τ_k, and $Q_E(\omega)$ is highly

nonlinear (see Appendix). Here, we use a simple grid search perturbation algorithm to determine the coefficients given a target Q_0. In general, any of a variety of nonlinear solution algorithms can be used to determine these coefficients, each having its own optimization criteria. Our fitting criterion seeks to minimize the sum of the squared residuals between $Q_E(\omega)$ and Q_0 over the prescribed absorption bandwidth. The approach used here results in a system that matches the target Q_0 reasonably well over about two decades in frequency (as shown below). Table 2 lists the coefficients for target Q_0 values of 5 and 2 determined with this technique for the ESM formulation. Figures 7, 8, and 9 show, respectively, the waveforms, apparent attenuation (Q_A), and phase velocity obtained from plane *P*- and *S*-wave calculations that use these optimized parameters. All other model parameters are the same as in previous tests.

For $Q_0 = 5$, an excellent fit is obtained between the theoretical and computed responses, with the measured Q_A matching the target Q_0 to within a few percent over roughly two decades of frequency. In Figures 8 and 9, we also show theoretical curves for $Q_E(\omega)$ and $c_E(\omega)$ to illustrate how the computed response closely follows the behavior predicted by the effective parameters. For $Q_0 = 2$, the fit to the theoretical response is still remarkably good, with the measured Q_A matching the target Q_0 to within a few percent over roughly one-and-a-half decades of frequency. Again, the effective parameters $Q_E(\omega)$ and $c_E(\omega)$ provide a reasonably accurate prediction of the behavior of the computed results.

It becomes increasingly difficult to derive a coarse-grain system that is valid over an appreciable bandwidth for Q values lower than about 2 because the $\bar{x}_k$ coefficients are very close to the stability limit (see Table 2). The only way to maintain stability for these very low Q values is to decrease the spread of the τ_k coefficients. In the limit that all the τ_k are equal, the coarse-grain system reduces to a narrow-band model with only a single memory variable (Robertsson *et al.*, 1994).

Table 2
Coefficients for Optimized Low Q_0 Models

	$Q_o = 5$		$Q_o = 2$	
k	$\bar{x}_k$	τ_k	$\bar{x}_k$	τ_k
1	0.700552	5.03655×10^{-3}	0.863550	4.48560×10^{-3}
2	0.666418	6.52579×10^{-3}	0.863550	4.48560×10^{-3}
3	0.609150	1.54751×10^{-2}	0.863550	4.48560×10^{-3}
4	0.602998	4.36147×10^{-2}	0.863550	1.78575×10^{-2}
5	0.567881	9.48709×10^{-2}	0.863550	1.78575×10^{-2}
6	0.609272	0.267383	0.863550	7.10919×10^{-2}
7	0.666418	0.753587	0.863550	0.224812
8	0.659820	1.94820	0.863550	0.252244

Layered Model Test

We test the performance of the coarse-grain formulations in more complex media (including a free surface) by running calculations for the three layer model listed in Table 3. A point double-couple with strike = 90°, dip = 90°, rake = 0°, and $M_0 = 10^{23}$ dyne·cm is used to initiate the calculations. The source depth is 2 km, and the moment rate function is a cosine-bell function given by

$$\dot{M}_0(t) = \begin{cases} \dfrac{M_0}{T}\,(1 - \cos 2\pi t/T), & \text{if } 0 \le t \le T; \\ 0, & \text{otherwise;} \end{cases} \tag{21}$$

with a width of $T = 0.2$ sec. The resulting time histories are analyzed for an observation point located 5 km from the source at an azimuth of 143°. The FD calculations use a grid spacing of 100 m, yielding a maximum frequency resolution of 1 Hz for a shear-wave sampling of 5 grid points per wavelength in the lowest velocity region of the model. In addition to the FD calculations, we also compute the solution using the frequency wavenumber (FK) technique. All results are low-pass filtered using a fourth-order, zero-phase Butterworth operator with a corner at 1 Hz.

First we compare the FD and FK results for a purely elastic (infinite Q) model. This comparison allows us to analyze the fidelity of the FD solution for the prescribed model parameters. Figure 10 plots the computed time histories and their associated Fourier amplitude spectra. The agreement between the FD and FK results is excellent in both the time and frequency domains. The only noticeable difference is a very slight delay of some of the later phases of the FD result, which can be attributed to the effects of numerical grid dispersion within the shallowest velocity layer.

Figure 11 compares the three coarse-grain FD formulations (Optimized ESM, ESM, and CM) with the FK result for the anelastic model. Obviously, the effects of anelasticity have a strong impact on the waveforms relative to the purely elastic case, most notably by reducing the overall amplitude of the signals and by suppressing much of the later arriving, shorter period energy. Both the Optimized ESM and ESM formulations do an excellent job of matching the waveforms and spectra of the anelastic FK result, demonstrating the ability of these formulations to accurately model very low (spatially variable) Q in the presence of sharp media boundaries and a free surface. In addition, the CM formulation performs reasonably well for this model. However this formulation tends to underpredict the amplitudes of the waveforms (particularly at shorter periods on the horizontal components) and exhibits a noticeable phase delay of the *S* waves and surface waves. These characteristics are consistent with the theoretical behavior of the CM formulation discussed earlier.

Discussion

The examples and theoretical analysis in the previous sections demonstrate the improved accuracy that is provided by the ESM formulation compared with the CM formulation, particularly for low Q values. From a practical standpoint,

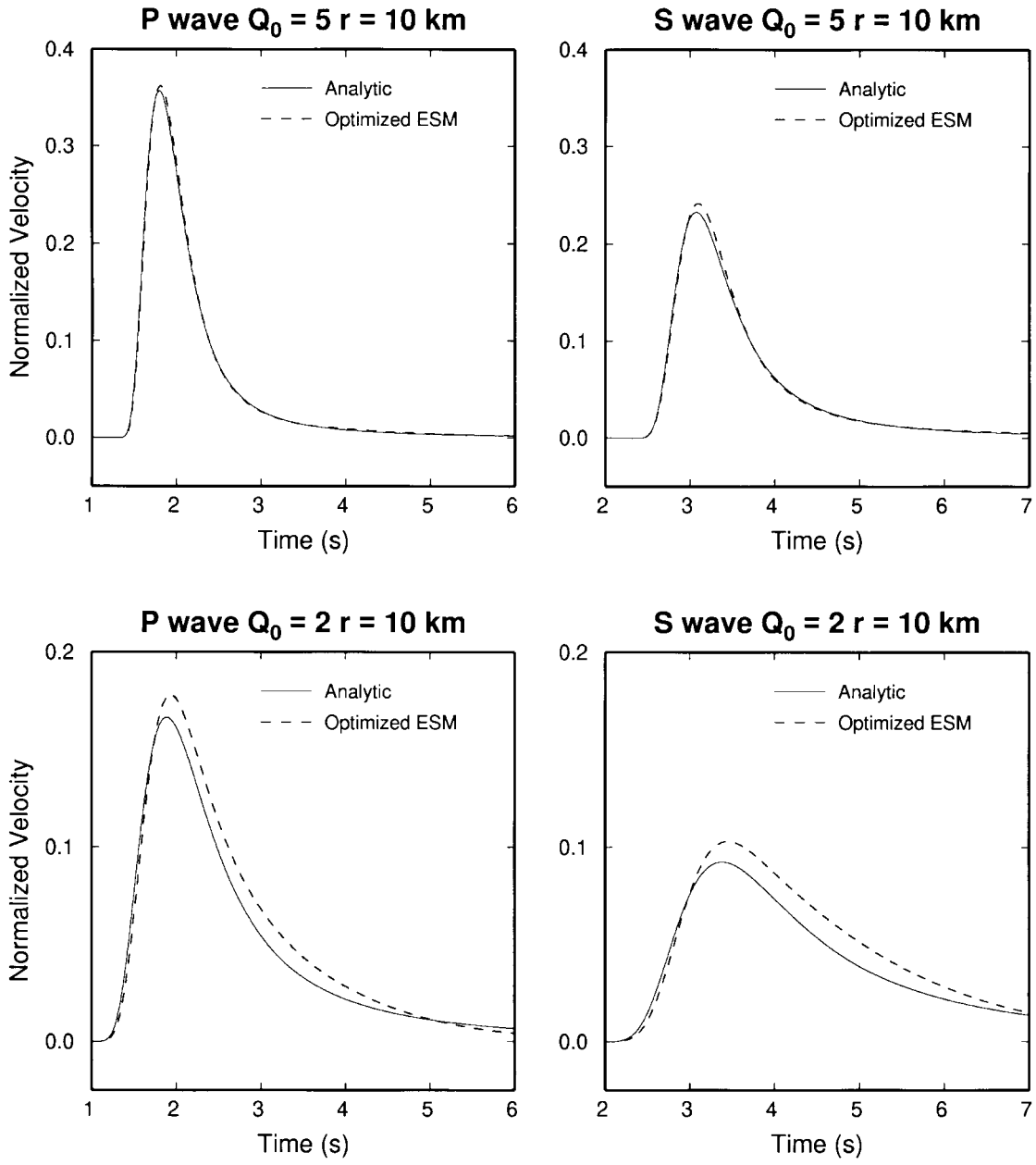

Figure 7. Waveform comparison for plane *P*-wave (left panels) and *S*-wave (right panels) calculations with target Q_0 values of 5 (upper panels) and 2 (lower panels). Propagation distance is 10 km. The analytic solution (solid line) is from Kjartansson (1979). For the coarse-grain calculation, the element-specific M_{k_u} solution (dashed line) uses equation (16) to specify the unrelaxed moduli, and the $\bar{x}_k$ and τ_k coefficients are determined using a grid search algorithm to optimize the fit of $Q_{\mathrm{E}}(\omega)$ to the target Q_0 value.

the implementation cost of the ESM formulation is virtually identical to the CM formulation (about 50%–60% increase in memory and CPU for either formulation relative to the purely elastic case). One possible exception to this is a model where the highest velocity material also has a very low Q, in which case the ESM formulation would require a smaller timestep than the CM formulation. Fortunately, for most applications the lowest Q values tend to strongly correlate with the lowest velocities, so the impact of this effect will generally be insignificant. In fact, for our layered model test, the timestep requirement was the same for the CM, ESM, and Optimized ESM formulations.

Our results also demonstrate that the Optimized ESM formulation can provide a high degree of accuracy for very low Q models. However, there are some issues concerning the general application of the optimized formulation that

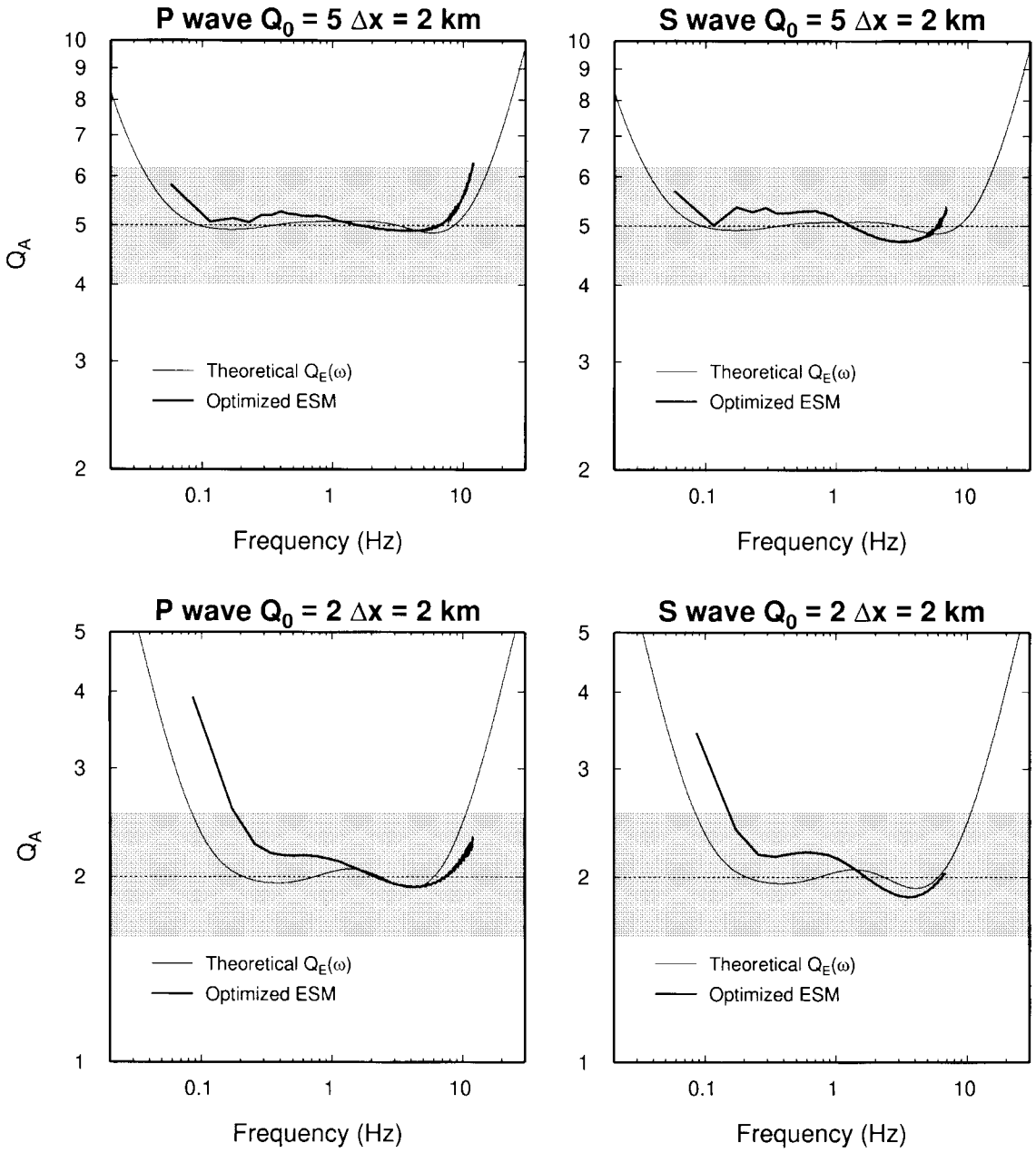

Figure 8. Apparent attenuation (Q_A) for the plane *P*-wave (left panels) and *S*-wave (right panels) calculations with target Q_0 values of 5 (upper panels) and 2 (lower panels). Separation distance is 2 km. The shaded region represents $\pm 25\%$ variation around the target Q_0 value. For the coarse-grain calculation, the element-specific M_{k_u} solution (thick line) uses equation (16) to specify the unrelaxed moduli, and the $\bar{x}_k$ and τ_k coefficients are determined using a grid search algorithm to optimize the fit of $Q_E(\omega)$ to the target Q_0 value. Also shown are theoretical $Q_E(\omega)$ curves determined from equation (A6).

warrant further discussion. First, the overhead cost associated with determining the optimized $\bar{x}_k$ and τ_k coefficients for a generally heterogeneous 3D model may be quite significant. For example, Olsen *et al.* (2001) have proposed a Q model for the Los Angeles basin that is proportional to the local seismic-wave velocity, which may be different at each grid point in the model. Optimization would require the calculation of the coefficients at each coarse-grain cell having a different Q_p and/or Q_s value. Some cost savings may be realized by precomputing and tabulating the coefficients for a limited number of reference Q values, and then assigning a reference value to each grid point. However, the practical benefit and accuracy of this type of approach needs further investigation.

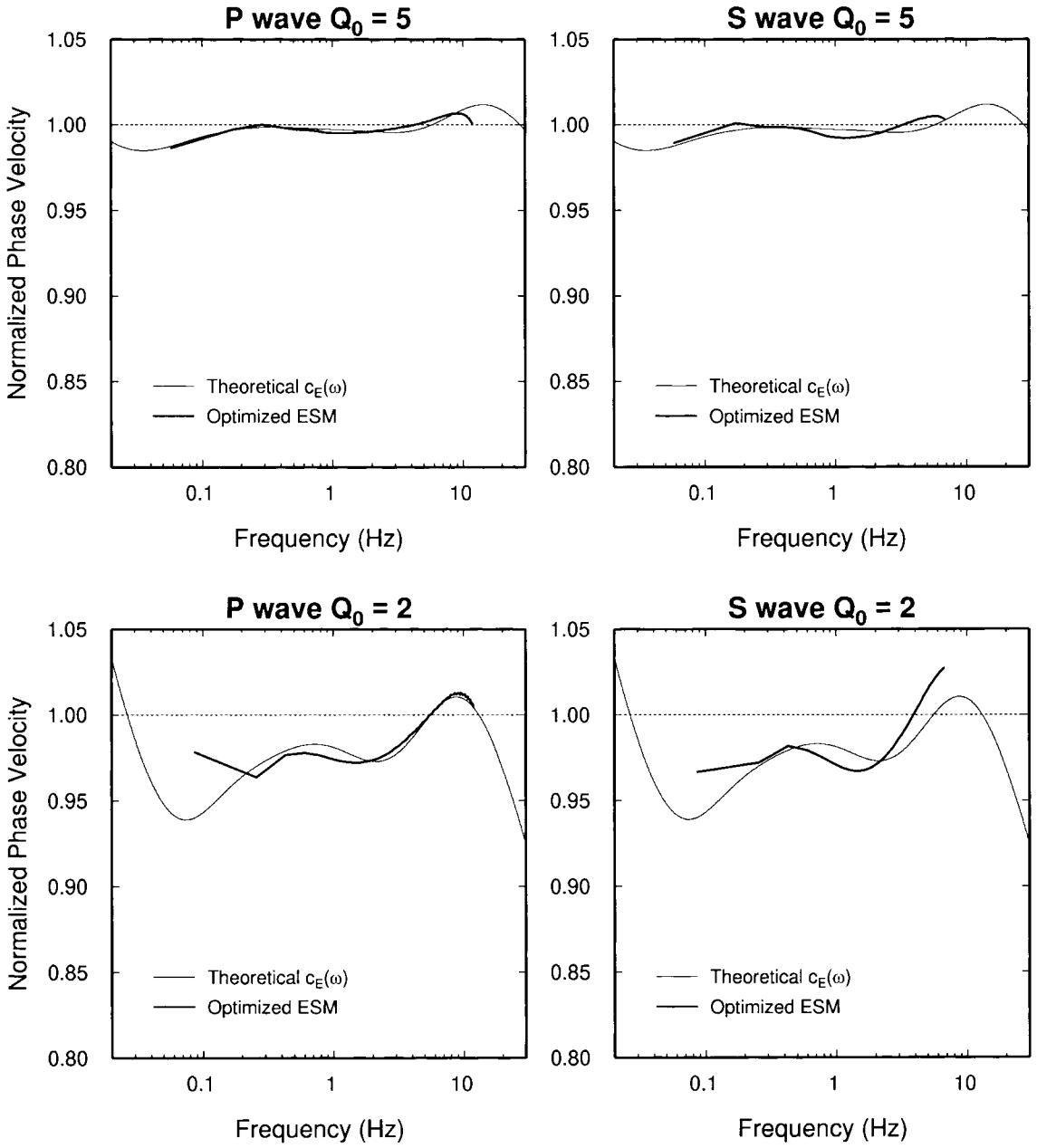

Figure 9. Normalized phase velocity measured from the plane *P*-wave (left panels) and *S*-wave (right panels) calculations with target Q_0 values of 5 (upper panels) and 2 (lower panels). For the coarse-grain calculations, the element-specific M_{k_u} solution (thick line) uses equation (16) to specify the unrelaxed moduli, and the $\bar{x}_k$ and τ_k coefficients are determined using a grid search algorithm to optimize the fit of $Q_E(\omega)$ to the target Q_0 value. Also shown are theoretical $c_E(\omega)$ curves determined from equations (15) and (A5).

Table 3
Layered Velocity Structure

V_p (km/sec)	V_s (km/sec)	Density (g/cm^3)	Q_p	Q_s	Thickness (km)
1.7	0.5	2.1	10	5	0.55
3.0	1.2	2.3	20	10	1.00
6.0	3.464	2.7	100	50	—

An additional issue is the trade-off between the added cost of optimization and the benefit of increased accuracy. Our layered model test indicates that there is not a significant difference in the performance of the optimized versus non-optimized versions of the ESM formulation even for models with Q values as low as 5. Most seismic applications fall into a class of models with $Q > 5$, and our results suggest that the non-optimized ESM formulation can easily handle

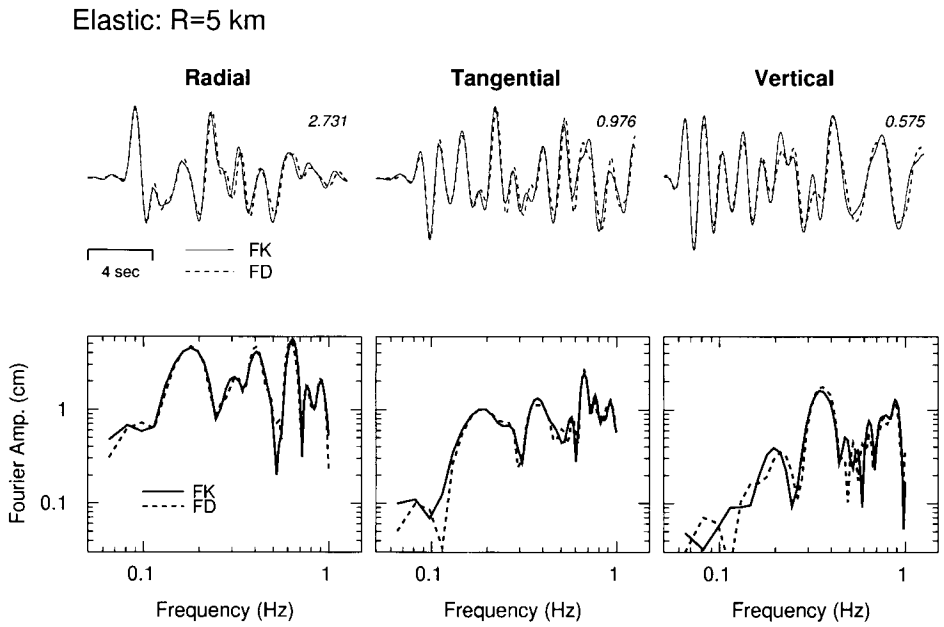

Figure 10. Comparison of FD and FK simulations for the purely elastic layered model test. Top panels show three component velocity waveforms at a range of 5 km from the source. Peak velocity for each component is indicated at upper right of each set of traces. Lower panels compare the Fourier amplitude spectra (unsmoothed) for the simulations. All results have been lowpass filtered at 1 Hz.

these applications with a very high degree of accuracy. For models with $Q < 5$ (e.g., shallow reflection applications; Xu and McMechan, 1998), optimized formulations may be used, or alternatively, the non-optimized ESM formulation can also be extended to very low Q values by reducing the range of the absorption band (see equation 14).

Another potential application involving very low Q is the suppression of artificial reflections in sponge zones adjacent to absorbing boundaries (Israeli and Orzag, 1981; Robertsson *et al.*, 1994). The broadband nature of the coarse-grain system allows for a more complete absorption of energy than the single memory variable scheme proposed by Robertsson *et al.* (1994) at no additional cost. For efficiency, we use the CM formulation in the sponge zone and gradually reduce the Q values to a minimum of $Q = 5$ right at the boundary. Although the CM formulation is less accurate than the ESM formulation, it requires a smaller value of the unrelaxed modulus, which consequently permits a larger timestep. This is an important consideration when high-velocity regions of the model lie along the computational boundary. The loss of accuracy in the sponge zone is of no practical significance since the goal is to remove this energy from the system anyway.

Although our present analysis only considers the case of frequency-independent Q, there is no theoretical reason that restricts the coarse-grain methodology to this special case. In the more general case [i.e., $Q = Q(\omega)$], the key to the coarse-grain formulation is determining the weighting coefficients ($\bar{x}_k$) that can reproduce the desired frequency behavior of the attenuation model. Unfortunately, unlike the constant Q_0 case, we are not aware of a simple analytic expression (such as equation 12) that can adequately represent the $\bar{x}_k$ when Q is frequency dependent. In this situation, it may be necessary to use a numerical procedure to solve for the $\bar{x}_k$ by fitting the $Q_E(\omega)$ to the desired $Q(\omega)$, such as that discussed earlier. The practical aspects of this approach are the subject of future study.

As a final point of discussion, we note that while most of the theoretical analysis presented here is based on simple models, our ultimate goal is to apply this technique to generally heterogeneous 3D media. In this case, each grid element may have different moduli and Q values. However, with the coarse-grain method, all elements of the coarse-grain cell (eight adjacent nodes in 3D) must have the same Q value (although they can still have different moduli). This effectively limits the spatial resolution of Q variability to twice the grid size. Previous studies have shown that harmonic averaging of the volumetrically normalized moduli provides the correct representation of internal media boundaries, even at the sub-grid level (e.g., Zahradník *et al.*, 1993; Graves, 1996; Moczo *et al.*, 2001). Following this approach, we calculate the target Q value for each coarse-grain cell by harmonically averaging the eight input Q values over the volume of the coarse-grain cell. This approach has worked very well in our test calculations (e.g. the layered model test); however, further evaluation is needed to more fully document the theoretical basis for this representation.

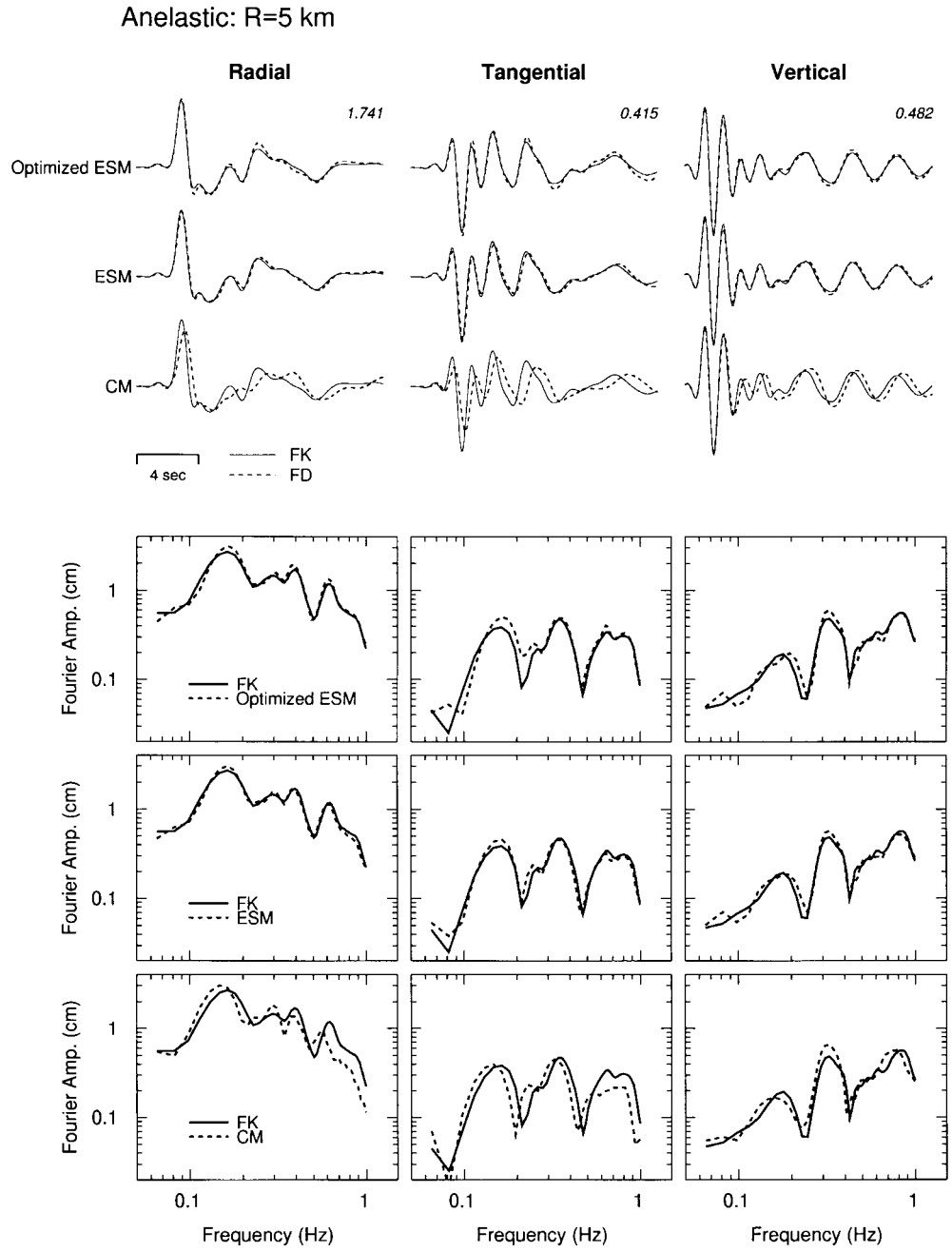

Figure 11. Comparison of FD and FK simulations for the anelastic layered model test. Three different FD simulations were performed, using respectively, the CM, ESM, and Optimized ESM formulations. Top panels show three component velocity waveforms at a range of 5 km from the source. Peak velocity for each component is indicated at upper right of each set of traces. Lower panels compare the Fourier amplitude spectra (unsmoothed) for the simulations. All results have been low-pass filtered at 1 Hz.

Conclusions

In this article, we provide a theoretical analysis of the stability and accuracy of the coarse-grain anelastic technique originally developed by Day (1998) and Day and Bradley (2001). We show that the behavior of the coarse-grain system is best described by effective parameters (M_E and Q_E) that are derived from the harmonic average of the moduli over the volume of the coarse-grain cell. The use of these effective parameters is essential for analyzing the performance and accuracy of the coarse-grain system, particularly for low values of Q. Our analysis derives a necessary stability condition for the coarse-grain system, which states that the weighting coefficients must lie between 0 and 1. Using the approach of Day and Bradley (2001) to specify the

weights satisfies this stability condition for Q values of about 3 and larger. However, using unconstrained optimization techniques will produce weights that violate this condition at much higher Q values. We also derive a modification of the original coarse-grain methodology called the element-specific modulus (ESM) formulation, in which each element of the coarse-grain cell has a different unrelaxed modulus. We demonstrate that the accuracy of the coarse-grain system for Q values lower than about 20 is significantly improved by using the ESM formulation. The cost of implementing the ESM formulation is virtually identical to the original Day and Bradley (2001) formulation. Finally, we present a technique for optimizing the accuracy of the coarse-grain system for very low Q models, based on matching the effective quality factor (Q_{E}). In addition, we demonstrate that using optimization techniques that do not employ the effective parameter Q_{E} will actually degrade (rather than improve) the accuracy of the resulting coarse-grain system.

Acknowledgments

The authors thank Jacobo Bielak and Shawn Larsen for their thoughtful and informative reviews of the original manuscript. Several of the figures for the manuscript were prepared using GMT software (Wessel and Smith, 1991). This work was sponsored in part by USGS External Program Grant 00-HQ-GR-0060 and funding from the Southern California Earthquake Center (SCEC). SCEC is funded by NSF Cooperative Agreement EAR-8920136 and USGS Cooperative Agreements 14-08-0001-A0899 and 1434-HQ-97AG01718. The SCEC contribution number for this article is 659.

References

Carcione, J. M., D. Kosloff, and R. Kosloff (1988). Wave propagation in a linear viscoacoustic medium, *Geophys. J. R. Astr. Soc.* **93,** 393–407.

Day, S. M. (1998). Efficient simulation of constant Q using coarse-grained memory variables, *Bull. Seism. Soc. Am.* **88,** 1051–1062.

Day, S. M., and C. R. Bradley (2001). Memory efficient simulation of anelastic wave propagation, *Bull. Seism. Soc. Am.* **91,** 520–531.

Day, S. M., and J. B. Minster (1984). Numerical simulation of attenuated wavefields using a Padé approximant method, *Geophys. J. R. Astr. Soc.* **78,** 105–118.

Graves, R. W. (1996). Simulating seismic wave propagation in 3D elastic media using staggered grid finite differences, *Bull. Seism. Soc. Am.* **86,** 1091–1106.

Emmerich, H., and M. Korn (1987). Incorporation of attenuation into time domain computations of seismic wave fields, *Geophysics* **52,** 1252–1264.

Israeli, M., and S. A. Orzag (1981). Approximation of radiating boundary conditions, *J. Comp. Phys.* **41,** 115–135.

Kjartansson, E. (1979). Constant Q wave propagation and attenuation, *J. Geophys. Res.* **84,** 4737–4748.

Liu, R., D. L. Anderson, and H. Kanimori (1976). Velocity dispersion due to anelasticity: implication for seismology and mantle composition, *Geophys. J. R. Astr. Soc.* **47,** 41–58.

Moczo, P., J. Kristek, M. Kristekova, and R. J. Archuleta (2001). Accuracy of the 3D finite-difference modeling of earthquake ground motion for real sites, Fall Meet. Suppl., *EOS Trans. AGU* 82, no. 47, Abstract S32D-10.

Olsen, K. B., C. R. Bradley, and S. M. Day (2001). Estimation of Q and near surface amplification for long-period waves in the Los Angeles basin, *Ann. Meet. Abstr. Seism. Res. Lett.* **72,** 283.

Robertson, J. O. A., J. O. Blanch, and W. W. Symes (1994). Viscoelastic finite-difference modeling, *Geophysics* **59,** 1444–1456.

Wessel, P., and W. H. F. Smith (1991). Free software helps map and display data, *EOS* **41,** no. 72, 441, 445–446.

Xu, T., and G. A. McMechan (1998). Efficient 3D viscoelastic modeling with application to near-surface land seismic data, *Geophysics* **63,** 601–612.

Zahradník, J., P. Moczo, and F. Hron (1993). Testing four elastic finite-difference schemes for behavior at discontinuities, *Bull. Seism. Soc. Am.* **83,** 107–129.

Appendix

Complete Expressions for M_E and Q_E

From equations (7) and (9) we can write

$$M_{\mathrm{E}}(\omega) = V_T\left\{\sum_{k=1}^{N}\frac{V_k}{M_{k_u}}\left[1 - \frac{\bar{x}_k}{\omega^2\tau_k^2 + 1} + i\,\frac{\bar{x}_k\omega\tau_k}{\omega^2\tau_k^2 + 1}\right]^{-1}\right\}^{-1}, \tag{A1}$$

where the element-specific unrelaxed modulus M_{k_u} is given by equations (16) and (17). Letting

$$\alpha_k = 1 - \frac{\bar{x}_k}{\omega^2\tau_k^2 + 1} \quad \text{and} \quad \beta_k = \frac{\bar{x}_k\omega\tau_k}{\omega^2\tau_k^2 + 1}, \tag{A2}$$

equation (A1) can be written as

$$M_E(\omega) = V_T\left\{\sum_{k=1}^{N}\frac{V_k}{M_{k_u}}\left[\frac{\alpha_k}{\alpha_k^2 + \beta_k^2} - i\,\frac{\beta_k}{\alpha_k^2 + \beta_k^2}\right]\right\}^{-1}. \tag{A3}$$

Now setting

$$A = \sum_{k=1}^{N}\frac{V_k}{M_{k_u}}\left[\frac{\alpha_k}{\alpha_k^2 + \beta_k^2}\right] \quad \text{and} \quad B = \sum_{k=1}^{N}\frac{V_k}{M_{k_u}}\left[\frac{\beta_k}{\alpha_k^2 + \beta_k^2}\right], \tag{A4}$$

we obtain the expression

$$M_{\mathrm{E}}(\omega) = V_T\left[\frac{A}{A^2 + B^2} + i\,\frac{B}{A^2 + B^2}\right]. \tag{A5}$$

Finally, from equations (8), (A4), and (A5), we have for the effective quality factor

$$Q_{\mathrm{E}}(\omega) = \frac{\displaystyle\sum_{k=1}^{N}\frac{V_k}{M_{k_u}}\left[\frac{\alpha_k}{\alpha_k^2 + \beta_k^2}\right]}{\displaystyle\sum_{k=1}^{N}\frac{V_k}{M_{k_u}}\left[\frac{\beta_k}{\alpha_k^2 + \beta_k^2}\right]}. \tag{A6}$$

URS Corporation
566 El Dorado Street
Pasadena, California 91101
robert_graves@urscorp.com
(R.W.G.)

Department of Geological Sciences
San Diego State University
San Diego, California 92182
day@moho.sdus.edu
(S.M.D.)

Manuscript received 21 March 2002.